Available online at www.sciencedirect.com
ScienceDirect
Journal of Catalysis 259 (2008) 5–16
JOURNAL OF CATALYSIS
www.elsevier.com/locate/jcat

Fuel cell performance and characterization of 1-D carbon-supported platinum nanocomposites synthesized in supercritical fluids

André D. Taylor *,[1], Ryan C. Sekol [1], Jeremy M. Kizuka, Salome D'Cunha, Craig M. Comisar

Department of Chemical Engineering, 2300 Hayward Street, University of Michigan, Ann Arbor, MI 48109, USA

Received 20 November 2007; revised 29 January 2008; accepted 31 January 2008

Available online 28 August 2008

Abstract

We present Pt particle size and fuel cell results for carbon black, carbon fibers, and single-walled carbon nanotubes (SWCNTs). The study investigated how high-temperature liquid and supercritical fluid synthesis conditions could influence the Pt particle size and fuel cell performance of these nanocomposite catalyst materials. High-temperature methanol is a suitable medium for Pt particle size deposition, generating smaller particles (90% measuring $\leqslant$5 nm). The addition of a surfactant, such as sodium dodecyl sulfate, to the fluid medium improved the fuel cell performance and Pt utilization of all 3 supports by 27 to 63%, with the best catalyst material, Pt/SWCNTs, having a peak power density of 449 mW/cm^2. This synthesis technique was a very fast (<5 min) process with no reactor sidewall effects on Pt particle size or yield.

Keywords: Fuel cells; PEM fuel cells; Supercritical fluids; Nanostructured catalysts; Carbon nanotubes; Carbon fibers

1. Introduction

There is growing interest in the development of high-performance fuel cell catalysts that have excellent Pt utilization and long-term durability [1–4]. The customary catalyst support for polymer electrolyte membrane (PEM) and direct methanol fuel cells is carbon black (CB) [5,6]. These low-cost materials offer reasonable surface areas and chemical resistance under fuel cell conditions (acidic and alkaline). A main drawback of conventional CB materials is the low utilization of precious metal catalyst caused by particle isolation, low ionomer-to-catalyst contact (triple phase boundaries), or inactive precious metal inside the inner pores [7]. Srinivasan et al. estimated this utilization to be as low as 10% [8,9]. Several groups have investigated the utility of 1-D carbon materials, such as carbon nanotubes (CNTs) [9,10] and carbon fibers (CFs) [11,12], in improving fuel cell performance. These materials can form the building blocks for sensors [13] and field effect transistors [14], and have been suggested as ideal scaffold supports for microbial fuel cells [15].

Although these 1-D carbon materials display promising mechanical and electrical properties for fuel cell applications, obtaining a homogeneous metal deposition on the hydrophobic inert surface is difficult [16–18]. Because CNTs are not wetted by liquids with surface tensions >0.1–0.2 N m^{-1}, traditional metal loading methods, such as wet impregnation, are not feasible [19]. Earlier methods of functionalization used surface modification, such as acid oxidation (e.g., HNO_3, $KMnO_4$, HNO_3/H_2SO_4, $K_2Cr_2O_7$) [20,21], UV/microwave treatments [22,23], and surface activation intermediates [24,25]. The harsh chemical and energy processing used to generate $=(O)_n$, $-(OH)_n$, $-(CO_2H)_n$, and other functional groups on the external surface can take more than 24 h of continuous controlled processing and generate aqueous wastes [26–28]. Extensive processing and functional groups can introduce defects and impurities into the support, decreasing fuel cell catalyst durability [2]. For instance, Deusberg et al. reported that hydrothermal treatment of single-walled CNTs (SWCNTs) at 500 °C in the presence of high concentrates of halides and sulfuric acid can lead to destruction of the nanotube structure [29].

Recently, several groups have investigated the use of supercritical fluids as an environmentally friendly medium for

* Corresponding author.
E-mail address: Andre.Taylor@yale.edu (A.D. Taylor).
[1] Present address: Department of Chemical Engineering, P.O. Box 208286, Yale University, New Haven, CT 06520-8286, USA.

0021-9517/$ – see front matter
doi:10.1016/j.jcat.2008.01.032

chemical reactions and separations [30–32]. For example, Park et al. reported the functionalization of CNT sidewalls by diluted nitric acid under supercritical conditions [33]. Ye et al. demonstrated nanoparticles of palladium, rhodium, and ruthenium (Ru) deposited on multiwalled CNTs (MWCNTs) through a hydrogen reduction of metal-β-diketone precursors in supercritical CO_2 and H_2 [34]. Lin et al. reported CNT-supported Pt and Pt/Ru nanoparticle catalysts synthesized in supercritical carbon dioxide using platinum(II) acetylacetonate $Pt(Acac)_2$ as the metal precursor [35,36]. Particle sizes ranged from 5 to 10 nm, and these were considered effective electrocatalysts for low-temperature fuel cells. They also used methanol-modified supercritical CO_2 reduction with H_2 using the same precursor. The addition of methanol modified the polarity of the CO_2 and improved dissolution of the $Pt(Acac)_2$ in the fluid phase [37]. Although no average particle sizes were provided, ranges were still too large (5–15 nm) for optimum efficiency of a fuel cell electrocatalyst (1–2 nm). To address this issue, Bayrakceken et al. used supercritical CO_2 and H_2 with dimethyl (1,5-cyclooctadiene) platinum(II) $PtMe_2COD$ (99.9%) to decorate nanoparticles onto MWCNTs [38]. They also demonstrated a Langmuir isotherm for this system with a maximum Pt loading of 15.2% and average particle size of 2.3 nm (45 particles). No fuel cell results or electrochemical analysis were reported in this work, and we note that before deposition, several steps were involved in processing the MWCNTs (i.e., heat treatment, 4 h; reaction chamber, 6 h; and N_2 reduction, 4 h).

Sun et al. described a slightly less complex approach using supercritical water in which Ru nanoparticles were deposited on the surface of CNTs at 400 °C for 2 h using $RuCl_3 \cdot H_2O$ as a precursor [39]. An average particle size of 5 nm was reported up to a 50% loading. This same group later described a method of loading Pt, Ru, Rh, and Sn nanoparticles onto CNTs using supercritical methanol [40]. The mean Pt particle size reported from TEM observation was 2–3 nm using $H_2PtCl_6 \cdot 6H_2O$ as a precursor. Under the reaction conditions of 300 °C, only 22% of the Pt precursor was reduced in 30 min. When this time was extended to 2 h, 100% of the precursor was reduced; however, the particle sizes agglomerated to 100 nm and/or fully covered the surface of the CNTs. Using the same Pt precursor and ethylene glycol as the reactant medium at 120 °C, Wang et al. exploited a salt effect that promoted selective heterogeneous nucleation of Pt nanoparticles onto the surface of CNTs [41]. By adding a salt such as sodium dodecyl sulfate (SDS) to the ethylene glycol solution, platinum nanoparticle sizes ranging from 2.3 to 9.6 nm were reported at a 50% loading. As is typical with nonsupercritical fluid methods, CNTs were refluxed at 120 °C in HNO_3 for 12 h, rinsed, and vacuum dried for 2 h, followed by oxidation in air at 550 °C for 30 min.

In previous work, we demonstrated how supercritical methanol could be used to create Pt-based catalysts on various CB supports (e.g., Black Pearls 2000, Monarch 700, XC-72). These catalysts were then dispersed into an ink solution that was deposited using ink jet technology to form 3-D catalyst layers with controlled composition and improved catalyst utilization [42]. We also loaded Pt onto the surface of 1-D carbon materials using either supercritical fluids [43] or selective heterogeneous nucleation [44]. The catalyst materials synthesized using both of these methods formed building blocks for free-standing fuel cell catalyst layers assembled using layer-by-layer self-assembly.

In the present work, we investigated the effect of supercritical fluid synthesis conditions on Pt nanoparticle size, loading, and fuel cell performance using CB (XC-72), SWCNTs, and CFs. Here we present fuel cell results for selected synthesis conditions using high-temperature methanol, supercritical methanol, and supercritical methanol with SDS. The solvation and reduction power of methanol to create fuel cell catalysts has not been described to date.

2. Experimental

2.1. Catalyst synthesis

Purified HiPco SWCNTs (impurities, 6–14%) were purchased from Carbon Nanotechnologies Inc. The catalytically grown CF material (Pyrograf III) was purchased from Pyrograf Products Inc. These tubular CFs are ca. 50 μm long, with an outside diameter of 50–200 nm and wall thickness of ca. 10 nm [45]. The CB (XC-72) was obtained from Cabot Corporation. All carbon supports were used as received.

A typical nanocomposite synthesis was performed by loading 35.0 mg of carbon support (CFs, SWCNTs, or CB), 87.5 mg of catalyst precursor (platinum acetylacetonate [$Pt(Acac)_2$]; Fisher Scientific), and an appropriate amount of MeOH into a 4.1-mL Swagelok reactor. This formulation resulted in a Pt/C catalyst with a nominal loading of 55 wt% Pt. The volume of MeOH varied based on the reaction temperature and target density. The reactor was sealed and heated in a preheated Techne SBL-2 sand bath. After soaking in the sand bath, the reactor was removed and cooled with forced air. SWCNT and CF composites were removed from the reactor and vacuum-filtered with a 1.0-μm Millipore Fluoropore membrane filter, washed multiple times with ethanol, and dried overnight in a fume hood. CB composites were not filtered, but instead were placed into a watch glass from which solvents were evaporated, with the sample dried overnight in a fume hood.

2.2. Catalyst synthesis with addition of SDS

The functionalization of the carbon support with SDS (Sigma–Aldrich) followed the procedure described in Section 2.1, with the modification of adding 2 wt% (54.0 mg) of SDS (based on the mass of all the reactants in the reactor). The SDS readily dissolved in the MeOH, and this addition promoted selective heterogeneous nucleation during the reaction [41].

2.3. Transmission electron microscopy

Transmission electron microscopy (TEM) was performed using a JEOL 3011 high-resolution electron microscope. TEM images and the public domain, Java-based image processing program, Image-J (Wayne Rasband, National Institute of Mental Health), were used to determine Pt particle size and count

on the surface of carbon supports. The particle counts for each sample ranged from 109 to 893, depending on the availability and contrast quality of the TEM images.

2.4. Cyclic voltammetry

Cyclic voltammograms (CVs) described the electrochemical activity of the catalysts by using a standard half-cell three-electrode setup with 0.5 M H_2SO_4 as the electrolyte and a Ag/AgCl reference electrode (Bioanalytical Systems). The catalyst was prepared on a glassy carbon electrode for the working electrode, with a Pt wire as the counter-electrode. Potential sweeps were made from −0.222 to 1.28 V using a Princeton Applied Research 273 potentiostat controlled by CorrWare software (Solartron Analytical). Before measurements, the system was purged with argon gas (99.999% pure, Cryogenic Gases) for periods ranging from 30 min to 2 h.

2.5. Catalyst loading

Thermogravimetric analysis (TGA), using a TA Instruments SDT Q600 analyzer, was used to determine the actual loading of the prepared catalysts as described previously [42,44]. In brief, experiments were conducted by increasing the sample temperature to 1000 °C. Steep reductions in mass were observed at approximately 420 °C, when the carbon support began to be consumed, leaving the Pt particles. At 1000 °C, it was assumed that all of the carbon support had been removed from the sample and that only oxidized Pt particles remained as platinum oxide (PtO). Catalyst loadings were calculated based on the initial mass of the platinum–carbon (Pt/C) nanocomposite and the final mass of the remaining PtO particles. Catalyst loadings determined by TGA also were verified by inductively coupled plasma analysis, using a Varian 710-ES optical emission spectrometer. In preparation for testing, catalyst samples were dissolved in aqua regia overnight and then diluted with deionized water. Analysis was performed against a range of five reference standards and compared with the theoretical concentration of the sample being evaluated.

2.6. Surface area analysis

Brunauer, Emmett, and Teller (BET) surface areas of carbon-supported nanocomposites were measured using a Micromeritics ASAP 2010 instrument. The catalyst samples were degassed at 350 °C until vacuum pressure was <5 μm Hg. The analysis was then performed under liquid nitrogen cooling at −195.79 °C (77.36 K).

2.7. MEA preparation and fuel cell testing

All prepared catalysts were used on the anode, whereas cathode catalysts were constructed with a standard Pt/CB catalyst (Alfa Aesar) with 20% Pt loading, unless noted otherwise. Anodic catalyst inks consisted of Pt/C (75 wt%) and Nafion (25 wt%), whereas the cathode ink consisted of Pt/C (68 wt%), Nafion (20 wt%), and polytetrafluoroethylene (12 wt%). All inks were mixed with equal parts of deionized water and isopropyl alcohol and stirred overnight to form good suspensions. Ink solutions were then hand-painted onto gas-diffusion layers (GDLs) and dried under vacuum for 5 min. The catalyst nanocomposite loading of all GDL paintings was targeted at 0.5 mg/cm^2. To form completed membrane electrode assemblies (MEAs), the anode GDL, cathode GDL, and a Nafion 117 membrane were hot-pressed together at 135 °C and 10 MPa for 5 min. Overnight conditioning for prepared MEAs was done in a single cell housing at 0.6 V with saturators set at 90 °C (100% relative humidity), O_2 and H_2 gas flow rates of 100 sccm, and a fuel cell temperature of 80 °C. Under steady-state current, an Agilent electronic load bank controlled cell potential and a National Instruments Data acquisition system controlled inputs during cell testing. LabView programs written exclusively for this fuel cell test station controlled and monitored the operation during each trial. The polarization curves displayed were not corrected for internal resistance. The Pt utilization (mW/mg$_{Pt}$) was determined by dividing the peak power density (mW/cm^2) by the anode catalyst loading (mg$_{Pt}$/cm^2).

3. Results and discussion

One objective of this work was to determine whether modifying the nanocomposite synthesis conditions (i.e., temperature, time, and fluid density) could control the Pt particle size. Table 1 gives a full summary of the experimental conditions and results. The run numbers shown in the first column identify each specific experiment, and the graph point in the second column illustrates the experimental conditions summarized in the subsequent columns and in Fig. 1. Variables in these experiments include the carbon support (i.e., CFs, SWCNTs, XC-72), temperature (°C), reaction time (min), fluid density (g/mL), isochoric pressure (MPa), and the methanol fluid medium (i.e., supercritical or high temperature). Results show the average particle size, standard deviation, and the percentage of particles ⩽5 nm. The Pt loading yield gives the percentage of Pt metal measured after synthesis out of the total amount of Pt available in the precursor. The nominal Pt loading for all experimental runs was 55 wt%. Selected synthesized catalyst materials were evaluated on the anode side of a PEM fuel cell with a standard cathode catalyst.

3.1. Catalyst characterization

Based on our previous work on ink jet printing [42] and layer-by-layer [43] fuel cell catalyst construction, we synthesized nanocomposites at 300 °C and a supercritical fluid density of 0.62 g/mL, shown as graph point A in Fig. 1. The average Pt particle size for CFs under these conditions was 3.4 nm (standard deviation ±2.4 nm), listed in Table 1 as run 1. From our observations, $Pt(Acac)_2$ was a better precursor compared with H_2PtCl_6 or $PtCl_2$, without the challenge of eliminating any chlorinated byproducts. The temperature of 300 °C is above the critical temperature of methanol (239.5 °C) and was adapted from the procedure described by Sun et al. [40]. Our first objective was to determine the quality of Pt particles attached to the

Table 1
Experimental conditions and results of nanocomposite synthesis

Run #	Fig. 1 graph point	Support	Temperature (°C)	Time (min)	Density (g/mL)	Pressure (MPa)	Reactor type	Fluid medium	Average particle size (nm)	Standard deviation (nm)	Particles ⩽5 nm (%)	Pt loading yield (%)	Peak power density (mW/cm^2)	Pt utilization (mW/mg_{Pt})
1	A	CF	300	30	0.62	85	SS	SC	3.4	2.4	84.7	78.6	334	609
2	B	CF	250	30	0.62	51	SS	SC	3.5	2.4	84.7	75.9		
3	C	CF	230	5	0.62	38	SS	HT	2.8	2.8	90.0	39.4	255	510
4	C	CF	230	30	0.62	38	SS	HT	3.4	3.0	84.6	71.1		
5	D	CF	200	30	0.52	4	SS	HT	4.5	4.0	71.8	48.2		
6	D	CF	200	90	0.52	4	SS	HT	4.5	5.9	80.7	55.6		
7	E	CF	230	30	0.41	7	SS	HT	3.0	3.6	85.1	74.3		
8	F	CF	250	30	0.29	10	SS	SC	4.5	4.8	75.8	82.6		
9	F	CF	250	30	0.29	10	SS	SC	4.3	5.6	81.8	75.7		
10	G	CF	300	30	0.29	17	SS	SC	4.2	4.5	79.2	68.1		
11	G	CF	300	30	0.29	17	Quartz	SC	4.5	5.9	79.1	78.9		
12	A	CF + SDS	300	30	0.62	85	SS	SC	3.1	2.6	88.8	81.7	393	775
13	A	SWCNTs	300	30	0.62	85	SS	SC	4.3	3.0	74.5	85.4	385	675
14	A	SWCNTs	300	60	0.62	85	SS	SC	4.4	2.9	72.5	77.8		
15	A	SWCNTs	300	90	0.62	85	SS	SC	4.7	3.3	73.4	70.6		
16	A	SWCNTs + SDS	300	30	0.62	85	SS	SC	4.5	3.4	65.2	78.8	449	919
17	A	SWCNTs	200	60	0.17	14	SS	SC $CO_2 + H_2$	6.9	4.3	38.6	87.2		
18	A	XC-72	300	30	0.62	85	SS	SC	4.5	4.1	70.2	85.4	243	493
19	A	XC-72 + SDS	300	30	0.62	85	SS	SC	3.0	2.1	89.0	77.0	426	802
20		JM catalyst							4.5	5.5	80.0	86.8	410	820

Note. CF—carbon fibers, SWCNTs—single walled carbon nanotubes, SDS—sodium dodecyl sulfate, SS—stainless steel, SC—supercritical methanol, HT—high-temperature methanol, JM—Johnson Matthey (HiSPEC 3000) Pt/carbon 20 wt%.

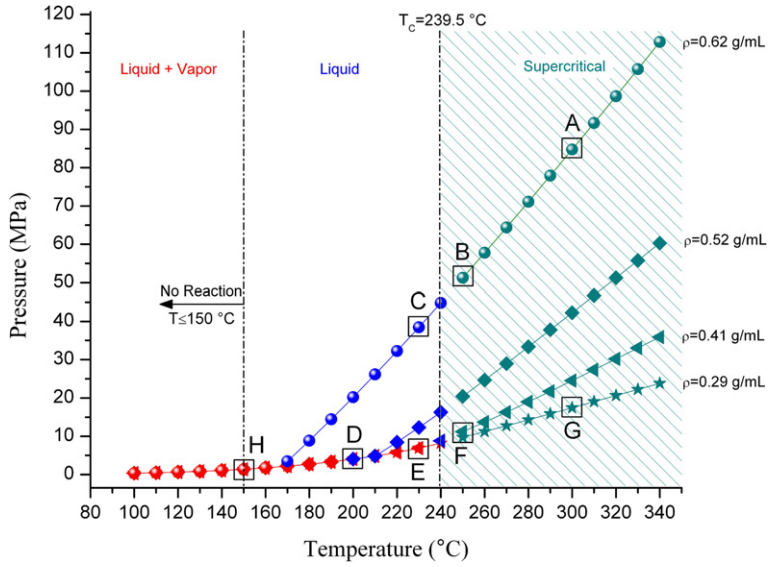

Fig. 1. Methanol pressure–temperature diagram illustrating the Pt/C nanocomposite synthesis conditions.

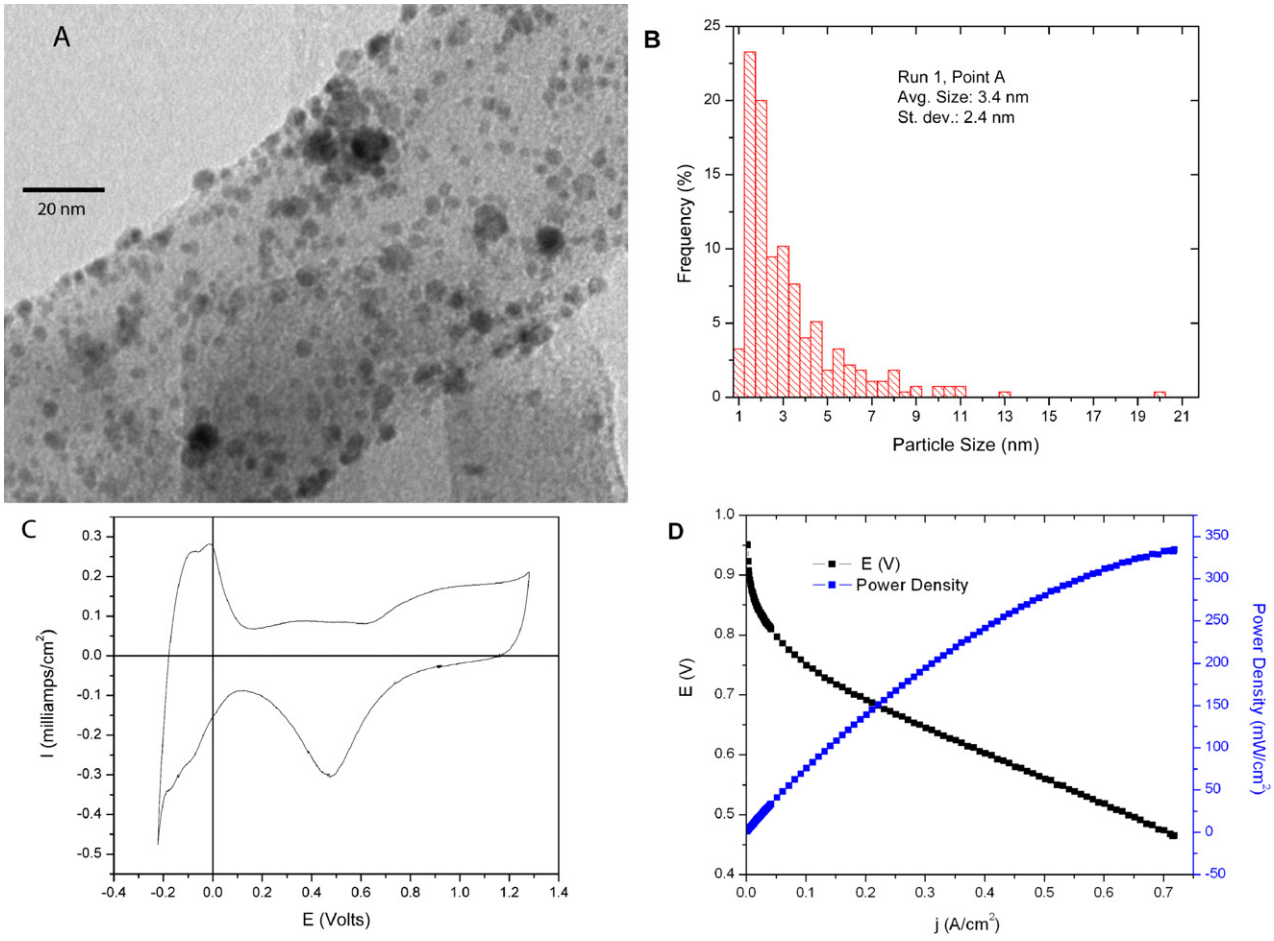

Fig. 2. (A–D) Pt on carbon fibers synthesized at 300 °C in 0.62 g/mL supercritical methanol. (A) TEM image, (B) particle size distribution, (C) cyclic voltammogram, (D) fuel cell polarization curve under the following conditions: fuel cell temperature 80 °C and saturators 90 °C, H_2 and O_2 flowrates 100 sccm, at 100% relative humidity.

support under this condition. Fig. 2 illustrates the TEM image, particle size distribution, cyclic voltammetry, and polarization curve of the Pt/CF material.

Particles on the CF surface were distributed evenly with a loading of 43.2 wt%, as shown in Fig. 2A. Fig. 2B illustrates the Pt particle size distribution. According to Table 1, 84.7%

of the particles were ⩽5 nm, below the range of 5–15 nm reported by Yen et al. [37]. Fig. 2C shows a cyclic voltammetry scan of the nanocomposite material demonstrating that the Pt was electrocatalytically active. In the potential range of 0.10 to −0.2 V versus the Ag/AgCl reference electrode, we noted the observation of pronounced H^+ adsorption and desorption peaks indicating that the Pt was fully reduced to a zero valence and was electrically attached to the CF surfaces. Fig. 2D shows the polarization curve with Pt/CFs as the anode catalyst at a loading of 0.55 mg_{Pt}/cm^2. The cathode was a standard JM catalyst (0.50 mg_{Pt}/cm^2). Run 1, as presented in Table 1, showed a peak power density for this material as 334 mW/cm^2, comparable with that of the standard JM catalyst (410 mW/cm^2), shown as run 20.

We noted that supercritical CO_2 and H_2 had been previously studied with $Pt(Acac)_2$ used as the precursor [35,36], and modified this setup in a batch process similar to one using methanol. In brief, a high-pressure syringe (ISCO model 260D syringe pump, Series D pump controller) was used to charge the reactor with 1:1 molar composition of CO_2 and H_2 to a pressure of 10 MPa. The reaction was carried out under supercritical conditions at 200 °C (14 MPa) for 1 h, listed as run 17 in Table 1. The best nanocomposite synthesis with supercritical CO_2 and H_2 was with SWCNTs. The average Pt particle size was 6.9 nm, with 38.6% of the particles <5 nm. This average value was more than double the average size of the Pt particles in run 1 (which used methanol), but was comparable to those reported by Lin et al. [35] (5–10 nm) using the same precursor. Lin et al. used a small amount of methanol as a modifier for the CNTs with CO_2 and H_2 at 200 °C. Our findings (runs 5 and 6) indicated that methanol could act as a reducing agent for $Pt(Acac)_2$ at 200 °C without the aid of H_2. In general, all methanol synthesis runs gave lower average particle sizes than the run with supercritical CO_2 and H_2.

3.2. Supercritical fluid comparisons

Fig. 3 illustrates selected TEM images and particle size distributions for graph points B, F, and G in Fig. 1. These comparisons were made at a reaction time of 30 min in a stainless steel reactor. Run 2 maintained the same fluid density (0.62 g/mL) as run 1, but with the temperature decreased from 300 to 250 °C. From Fig. 1, this synthesis (shown as point B) was still within the supercritical regime, but just above the supercritical temperature. Lowering the temperature from point A to point B decreased the pressure from 85 to 51 MPa. The average Pt particle size at point B was 3.5 ± 2.4 nm, comparable to that of run 1. At a fluid density of 0.62 g/mL between 250 and 300 °C, the temperature had little effect on the Pt particle size or yield. Points F and G represented the same temperature comparison at a lower fluid density of 0.29 g/mL. The average particle sizes for point F in runs 8 and 9 were 4.5 and 4.3 nm, respectively. Runs 8 and 9 illustrate the reproducibility of two different Swagelok reactors under the same experimental conditions. Averaging both particle size runs to 4.4 nm, this value was higher than the 3.5 nm of run 2 (point B) at the same temperature (250 °C) and reaction time. At 300 °C, run 1 (point A) and run 10 (point G) also had a similar difference in size, at 3.4 and 4.2 nm, respectively. These findings indicate that density at a higher regime could minimize the Pt particle size for synthesis on CFs. The standard deviations of the Pt particles also had a wider distribution (∼ twice as large) at the lower fluid density, as can be seen by comparing the first and second rows of Fig. 3 for 250 °C. In general, the Pt loading yield was independent of temperature and fluid density in the supercritical regime, which averaged ∼80%.

3.3. Wall reactions

Runs 10 and 11 of point G provide a comparison between the stainless steel (SS) and quartz (Q) reactors to investigate reactor sidewall effects. (It was not possible to make this comparison at graph points A and B, due to the limitations of quartz at high pressures.) Both sets of reactions were at 300 °C for 30 min with a MeOH fluid density of 0.3 g/mL (17 MPa). The average particle sizes were 4.2 nm (SS) and 4.5 nm (Q). The SS reactor had a smaller standard deviation compared with the Q reactor (4.5 nm vs 5.9 nm). We believe that this deviation was due to the radial difference in the smaller Q reactors (2 mm i.d.), with four Q reactors needed to make up the same volume as one SS reactor. Due to this finding, we carried out the remaining experiments using the stainless steel reactors, which were easier to load, seal, and open. Pt deposition on the inside walls was observed from the quartz reactions.

3.4. High-temperature fluid comparisons

We investigated whether any dramatic effect on Pt particle size occurred outside of the supercritical regime. Runs 3–7 (Table 1), corresponding to graph points C, D, and E, represented the high-temperature methanol regime as a hot compressed liquid. The particle size result of run 4 (point C) at 230 °C was comparable to that of run 2 (point B) at 250 °C, on opposite sides of methanol's critical temperature at the same fluid density of 0.62 g/mL. The average particle size for run 3 was 3.4 ± 3.0 nm. The particle size of run 4 (point C) was very close to those of run 1 (point A) and run 2 (point B). Run 7 (point E) was conducted at the same temperature as run 4 (point C) but at a lower fluid density (0.41 g/mL). The average particle size for point E was 3.0 ± 3.6 nm, lower than the 4.5 nm obtained for run 8 (point F), just across the critical temperature line. Run 7 (point E) was in the liquid + vapor phase just below the critical temperature, which appeared to maximize nucleation sites and suppress particle size growth.

The lower limit of the methanol reaction temperature was investigated at 200 °C, shown as point D (run 5). The average Pt particle size was 4.5 ± 4.0 nm. This value was comparable to the lower-density supercritical experiments listed as point F (runs 8 and 9) and point G (run 10). No reaction was observed at 150 °C (point H). Compared with point D (run 5), point E (run 7) was in the hot compressed liquid + vapor phase at 230 °C. For point D (200 °C), the Pt loading yield was only 48.2% of the expected amount, compared with 74.3% for

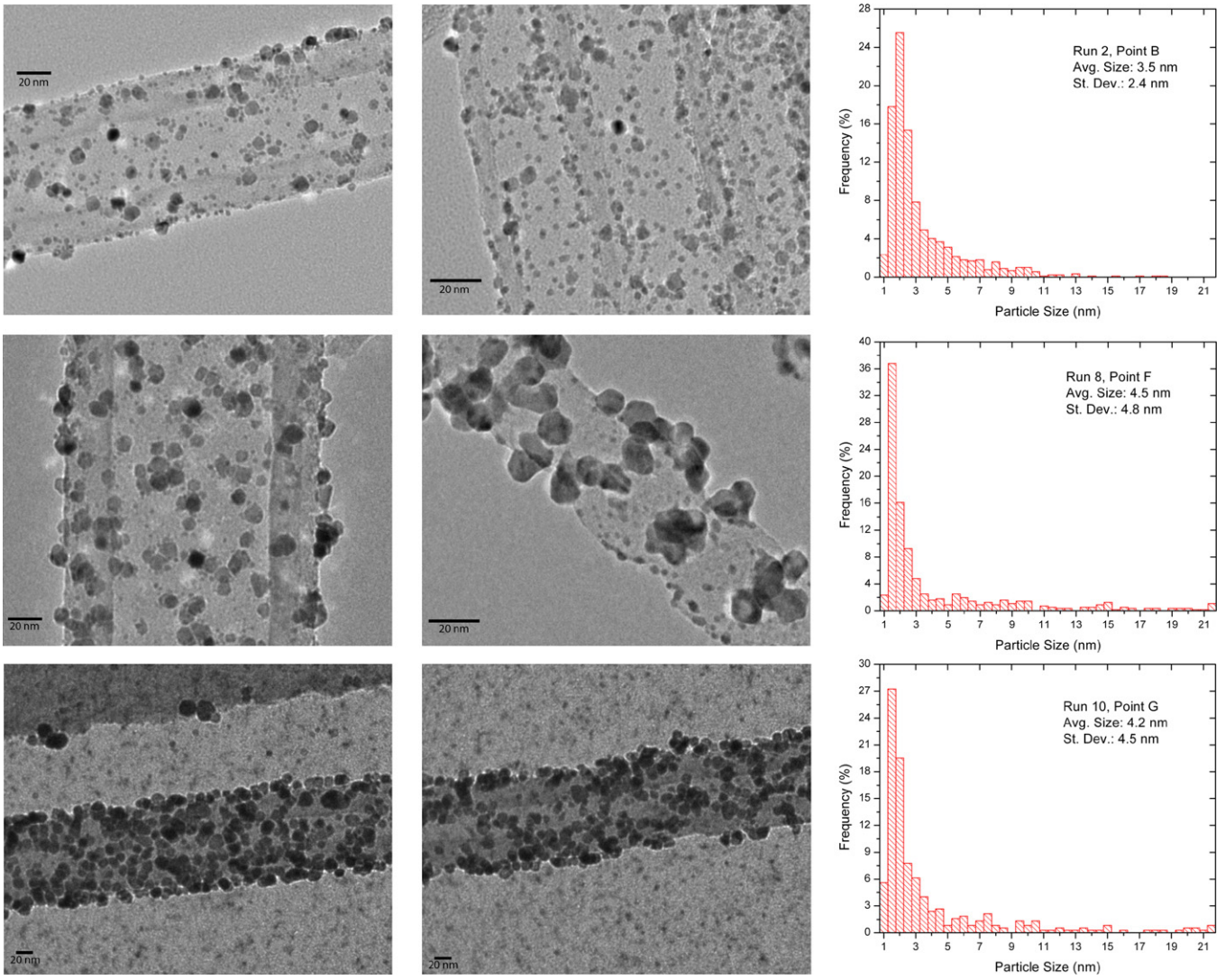

Fig. 3. Top row: Pt on carbon fibers (point B) synthesized at 250 °C in 0.62 g/mL supercritical methanol. Middle row: Pt on carbon fibers (point F) synthesized at 250 °C in 0.29 g/mL supercritical methanol. Bottom row: Pt on carbon fibers (point G) synthesized at 300 °C in 0.29 g/mL supercritical methanol.

point E (230 °C), but Pt particle sizes were 4.5 and 3.0 nm, respectively. With relatively close densities and pressures, these results suggest that the temperature should be high enough to promote a sufficient number of nucleation sites for the precursor, and that the solution phase could play a significant role in particle growth.

3.5. Time effects

We compared selected runs to evaluate the effects of reaction time on the Pt size and yield of synthesized nanocomposites. High-temperature methanol (point D), shown in Table 1 as runs 5 and 6 (200 °C), compared CFs at reaction times of 30 and 90 min, respectively. The 2 runs illustrated in Fig. 4 demonstrated comparable final properties, with an average particle size of 4.5 nm (but standard deviation of 5.9 nm for run 6 and 4.0 nm for run 5). The yield (slightly higher [∼7%] for run 6) suggests that the material contributed to the existing particles and also created newer, smaller particles, thereby maintaining the average and widening the standard deviation. For SWCNTs (runs 13–15), particle size grew with increasing reaction time, from 4.3 nm for 30 min to 4.4 nm for 60 min and finally 4.7 nm for 90 min. We attempted to correlate this size with our measured yield; however, the yield showed a reverse trend. We have no explanation for this finding, except that maybe the larger particles did not remain attached to the surface of the SWCNTs as the smaller ones did. We note that the SWCNTs and CFs both contained ∼7 wt% metal impurities, based on TGA measurements of as-received material.

At very short reaction times (e.g., 5 min), SWCNTs functionalized using supercritical methanol (300 °C, 0.62 g/mL) exhibited pyrophoric properties. Removal from the reactor and contact with air resulted in autoignition of the material, leaving only sintered nonviable catalyst. Pyrophoricity suggested that 5 min was not sufficient for the reactants to become fully reduced. No degradation was observed for CFs under the same conditions. We believe that this outcome was due to the drastically different surface areas measured in the materials. The BET surface areas before and after Pt loading were 610 and

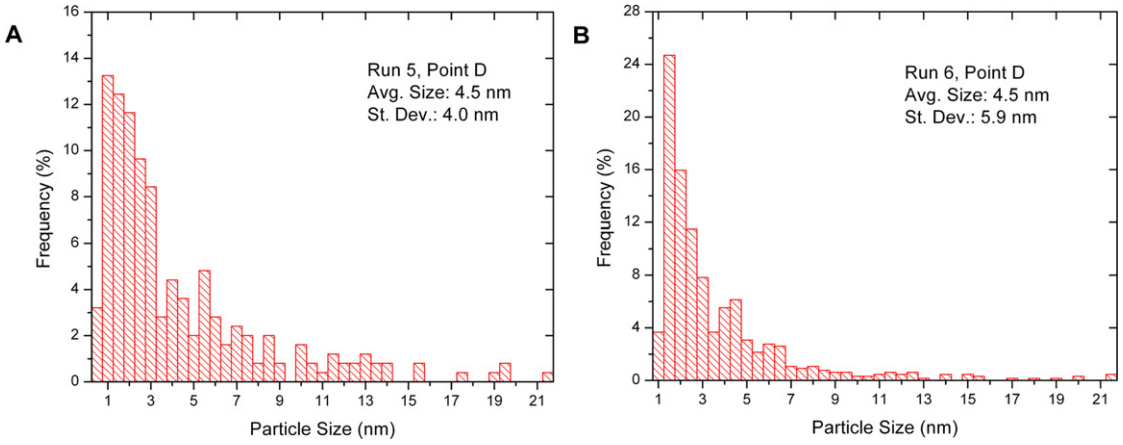

Fig. 4. (A) The particle distribution of run 5 and (B) the particle distribution of run 6.

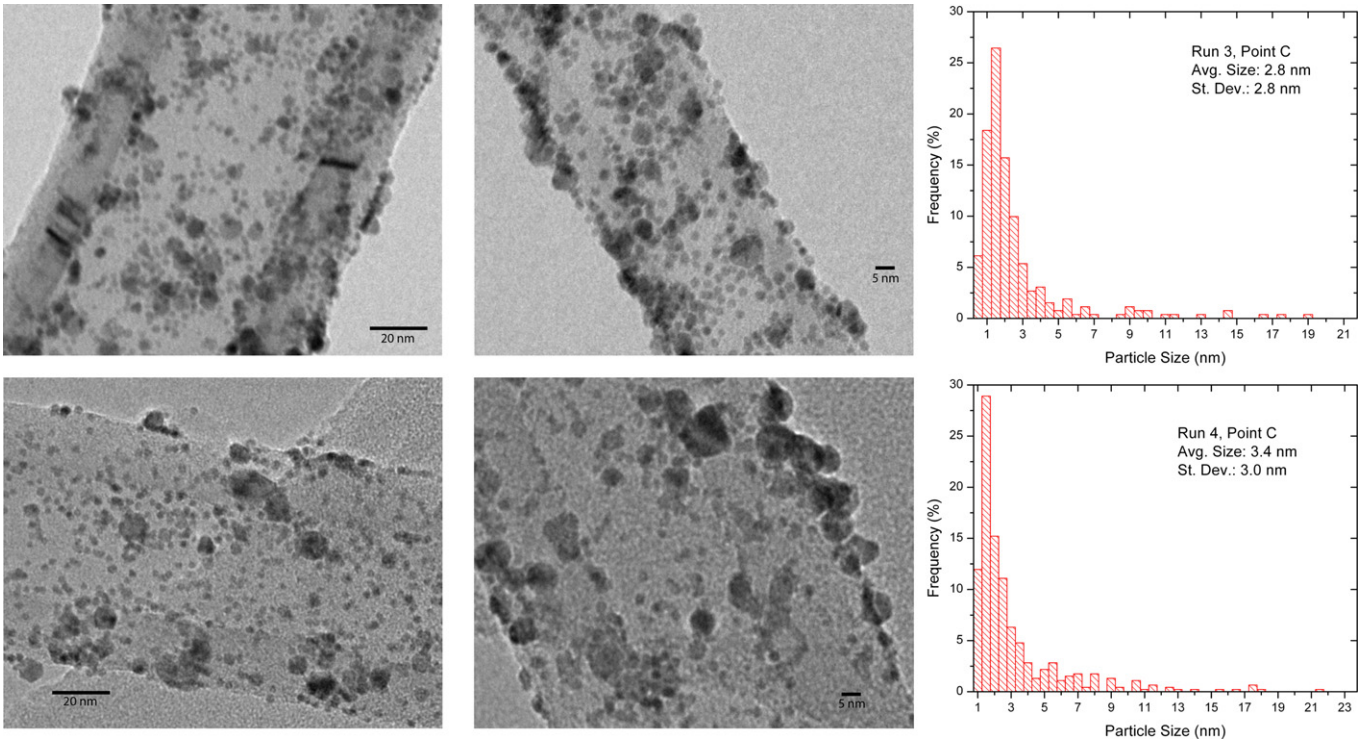

Fig. 5. Pt on carbon fibers (point C) synthesized at 230 °C in 0.62 g/mL supercritical methanol. Top row: 5 min (run 3), bottom row: 30 min (run 4).

400 m^2/g for SWCNTs, 41 and 30 m^2/g for CFs, and 229 and 181 m^2/g for XC-72.

Runs 3 and 4 (point C in Fig. 1) were used to estimate how fast the reduction of the Pt precursor was taking place. Fig. 5 shows the corresponding micrographs and particle size distribution. Lin et al. suggested that the reduction of Pt^{2+} to Pt^0 occurred within only 15 min for $Pt(Acac)_2$ in supercritical CO_2 and H_2 [35]. The reactor for run 3 was placed in the sand bath for 5 min under the same temperature and density conditions as used in run 4 (230 °C, 0.62 g/mL). The average particle size for run 3 was 2.8 ± 2.8 nm. To the best of our knowledge, 2.8 nm is the lowest value reported in the literature for Pt nanoparticle synthesis using high-temperature methanol. The count for this average was 261 particles, with 90% ⩽5 nm. At 30 min (run 4), the average Pt particle size was 3.4 ± 3.0 nm. The reduction and nucleation of Pt^{2+} to Pt^0 was quite fast in high-temperature methanol, but the Pt loading yield was approximately 39.4% (of the 55 wt% nominal loading), compared with 71.1% found under the same conditions at 30 min. Taking the ratio of the Pt loading yields of runs 3 and 4 (39.4/71.1), we get a material ratio of 55.4%. Assuming that the Pt particles were perfect spheres with an average radius of 1.4 nm in run 3 and 1.7 nm in run 4, we can calculate the mass ratio of run 3 to run 4 as 55.9%. This finding suggests very fast nucleation of the Pt particle sites, with the remaining precursor material contributing to the growth of existing particles. Fig. 5 shows that the density of particles on the surface of the CFs was similar but that run 3 had smaller particles and a tighter distribution than run 4.

We constructed a model simulation of the Swagelok reactor to further investigate the results of run 3. We used this model

Table 2
Methanol properties, values/expressions used in the simulation [46,47]

Property	Value/expression	Units
Thermal conductivity (isotropic)	$0.2837 - 0.000281T$	W/(m K)
Density	293.037	kg/m^3
Heat capacity	$(105800 - 362.23T + 0.9379T^2)/32.04$	J/(kg K)

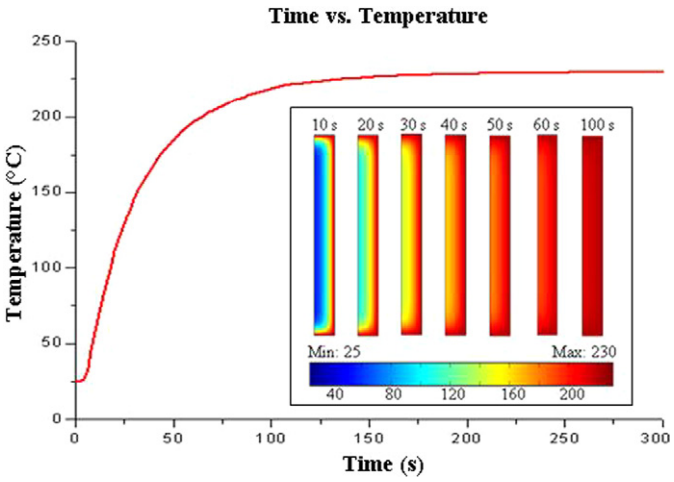

Fig. 6. Time (s) vs temperature (°C) of the Swagelok reactor contents. The inset image shows the changing temperature gradient at different time intervals during the simulation.

to estimate whether the contents of the reactor reached the desired temperature (230 °C) within 5 min. A 2D axial symmetric conductive heat transfer model was run using Comsol Multiphysics software. The methanol fluid and stainless steel reactor properties are given in Table 2 [46,47]. Fig. 6 shows that the reactor contents reached 230 °C within 5 min. The inset shows the temperature gradient on half of the vertical cross-section of the reactor at different time sets. According to the simulation, the contents were 200 °C at 64 s (1.1 min) and 220 °C at 104 s (1.7 min), and 230 °C at 210 s (3.5 min). These findings closely correspond to the experimental observations of Lawson and Klein, who suggested a heat-up time on the order of a few minutes using a similar reactor and sandbath setup [48].

Fig. 7 illustrates the activity of the Pt/CF nanocomposite synthesized at 5 min (run 3) as the anode catalyst at a loading of 0.50 mg$_{Pt}$/cm^2. Looking at the top row of Fig. 5 (run 3), we can see that the particles on the surface of the CFs were evenly distributed with a loading of 21.7 wt% (55 × 0.394). The cathode was a standard JM catalyst (0.50 mg$_{Pt}$/cm^2). The peak power density for this material (run 3) was 255 mW/cm^2. This value is lower than that for CFs functionalized under supercritical conditions (300 °C, 0.62 g/mL), shown as run 1 (334 mW/cm^2), possibly due to the lower Pt loading of the Pt/CF catalyst.

3.6. Addition of SDS surfactant

To investigate the influence of the surfactant as a mediator for selective heterogeneous nucleation [41], we added 2 wt% SDS to the reactor during preparation of the Pt/C nanocomposites. While mixing the contents before the reaction, we noted that the SDS readily dissolved in the methanol. For these comparisons, we selected the supercritical conditions shown in Fig. 1 as point A (300 °C, 0.62 g/mL). We compared the results for the CFs in run 1 (no SDS) and run 12 (with SDS). The 2 runs displayed similar particle sizes (3.4 and 3.1 nm) and Pt loading yields (78.6 and 81.7%). The standard deviations were also similar (2.4 and 2.6 nm). For run 1, 84.7% of the Pt particles were ⩽5 nm; for run 12, this figure was 88.8%. The percentages of particles ⩽5 nm were higher in runs 1 and 12 than in any other run except run 3. The primary difference between the 2 catalyst materials in runs 1 and 12 appears to be the quality of available Pt particles. This difference was demonstrated by fuel cell test results (Fig. 8D) showing a marked increase in peak power density and Pt utilization. The Pt/CF nanocomposite synthesized with SDS provided a peak power density of 393 mW/cm^2 in run 12 versus 334 mW/cm^2 in run 1 for a non-SDS Pt/CF catalyst. The Pt utilizations recorded for the same comparison were 775 mW/mg$_{Pt}$ for run 12 and 609 mW/mg$_{Pt}$ for run 1, an increase of 27%.

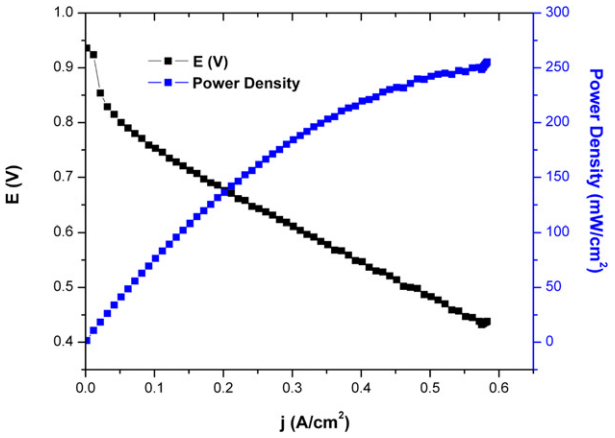

Fig. 7. Fuel cell polarization and power density curves of Pt on carbon fibers synthesized at 230 °C in 0.62 g/mL supercritical methanol for 5 min. Fuel cell temperature 80 °C and saturators 90 °C, H_2 and O_2 flowrates 100 sccm, at 100% relative humidity.

Runs 13 and 16 compared SWCNTs under the same conditions (300 °C, 0.62 g/mL) with and without SDS. Fig. 9A illustrates this comparison with polarization and peak power density curves. Particle sizes were 4.3 ± 3.0 nm for the Pt/SWCNT without SDS and 4.5 ± 3.4 nm for the Pt/SWCNT with SDS. Even though its Pt particle sizes were slightly larger, the Pt/SWCNT with SDS material gave a peak power density of 449 mW/cm^2, representing a ∼17% increase in performance over the Pt/SWCNT without SDS, with a peak power density of 385 mW/cm^2. The highest Pt utilization value found was 919 mW/mg$_{Pt}$, for Pt/SWCNT with SDS; this represents an increased Pt utilization of 36% (up from 675 mW/mg$_{Pt}$). The addition of SDS to the reactor had a more pronounced affect on performance when XC-72 was used as a support. The peak power density for the Pt/XC-72 without SDS was 243 mW/cm^2, and that of Pt/XC-72 with SDS was 426 mW/cm^2. This indicates a 75% increase in the performance of this catalyst material from adding SDS to the reactor.

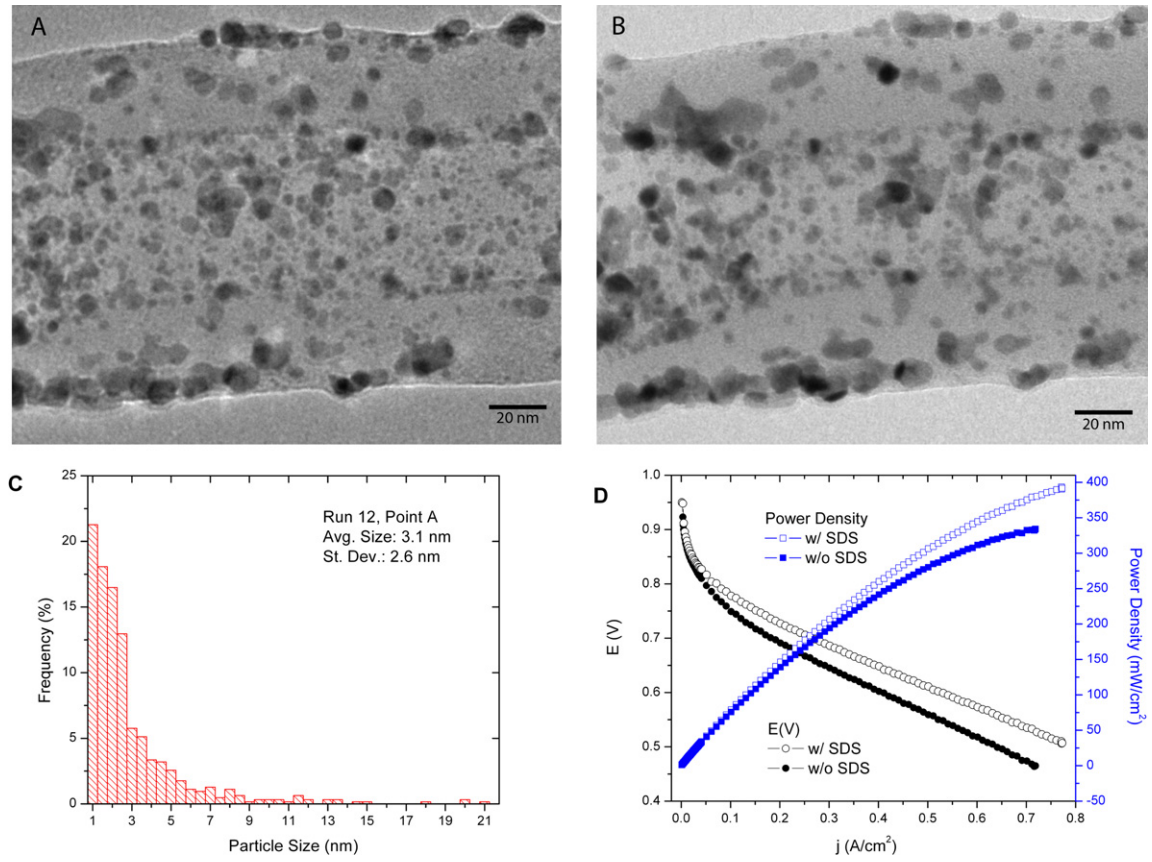

Fig. 8. (A–D) Pt on carbon fibers synthesized at 300 °C in 0.62 g/mL supercritical methanol with addition of SDS. (A) TEM image, (B) TEM image, (C) particle size distribution, (D) fuel cell polarization curve under the following conditions: fuel cell temperature 80 °C and saturators 90 °C, H_2 and O_2 flowrates 100 sccm, at 100% relative humidity, where outlined points symbolize with SDS (outlined points) and without SDS (solid points).

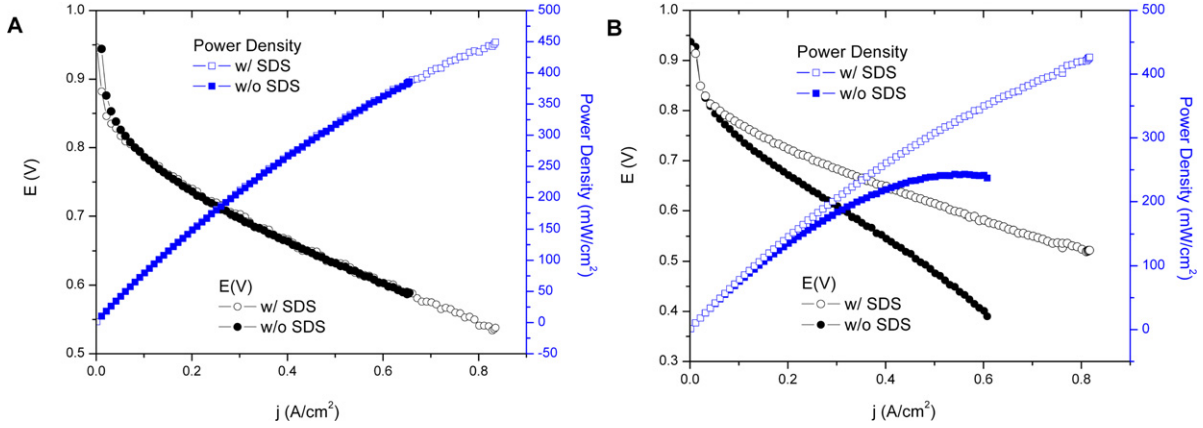

Fig. 9. Fuel cell polarization curves under the following conditions: fuel cell temperature 80 °C and saturators 90 °C, H_2 and O_2 flowrates 100 sccm, at 100% relative humidity. (A) A comparison of SWCNTs with SDS (solid points) and without SDS (outlined points), (B) a comparison of XC-72 with SDS (outlined points) and without SDS (solid points).

Pt utilization also rose from 493 mW/mg_{Pt} to 802 mW/mg_{Pt}, an increase of 63%. Note that the Pt particle size of the Pt/XC-72 (w/SDS) was 3.0 ± 2.1 nm, compared with 4.5 ± 4.1 nm for the Pt/XC-72 without SDS. The standard deviation for the Pt/XC-72 with SDS was the smallest found in this study. We also found that 89% of the Pt particles were ⩽5 nm in the Pt/XC-72 with SDS, compared with 70.2% in the Pt/XC-72 without SDS.

Wang et al. speculated that the presence of a metal salt (e.g., SDS) in the reaction solution either decreases the activation barrier toward heterogeneous nucleation or increases that toward homogeneous nucleation [41]. In the absence of SDS, only a small amount of Pt nanoparticles on CNTs was observed [41]. From our experimental observations, the Pt loading yield remained close to the same value for CFs without SDS (78.6%) and CFs with SDS (81.7%). The Pt loading yield ac-

tually decreased by 6.6% for the SWCNTs and by 8.4% for XC-72 when SDS was used. This seems to suggest that higher quality Pt nanoparticles were produced on each carbon support when using SDS. Little data are available on the micellar aggregation of SDS in methanol. Jacquier et al. reported a critical micelle concentration (CMC) of SDS in 35% (v/v) methanol of $\sim 8 \times 10^{-3}$ M [49]. The CMC trend showed a positive slope, with $\sim 5.2 \times 10^{-3}$ at 0% (v/v) methanol [49]. For our experiments, the SDS concentration for 2 wt% was 6.0×10^{-2} M using 100% methanol. According to Emerson and Holtzer [50], methanol is a less effective denaturant (i.e., micelle breaker) compared with glycerol or ethylene glycol. Based on these observations, we speculate that the concentration of SDS in our reactor was above the CMC level. Thus, the presence of micelles in the protic solvent could affect the initial attachment of the Pt particles on the surfaces of the carbon support, leading to an improved Pt nanoparticle.

4. Conclusion

We have demonstrated a simple approach to decorating 1-D carbon supports with platinum, which exhibit high performance for PEM fuel cell applications. CB, CFs, and SWCNTs were functionalized in a single-vessel batch reaction, using methanol as the reaction medium. These materials were characterized and showed promising catalytic properties in PEM fuel cells. This functionalization process reduced the need for harsh pretreatments of the carbon supports, decreasing the time and cost of synthesis. This approach also has implications for improved fuel cell catalyst durability. Under supercritical conditions, we found that higher fluid densities suppressed the average particle growth size from ∼4.3 to 3.4 nm for CFs and dropped the standard deviation from ∼5.0 to 2.4 nm. By lowering the temperature to 230 °C (just below the critical temperature of methanol), we have shown for the first time that high-temperature methanol can be a viable method of synthesizing fuel cell catalysts. Active Pt/CF fuel cell catalysts synthesized under these conditions showed an average particle size of 2.8 ± 2.8 nm, with 90% of the particles $\leqslant 5$ nm. We also have demonstrated the benefit of using a surfactant (in this case, SDS) in the synthesis of Pt nanoparticles in supercritical methanol. Catalysts created in this fashion showed comparable Pt nanoparticle structures based on high-resolution TEM imaging but demonstrated superior PEM fuel cell activity, with increases in platinum utilization as high as 27% for Pt/CFs, 36% for Pt/SWCNTs, and 63% for XC-72. Pt/SWCNT catalysts synthesized in supercritical methanol with SDS had the best performance, with a peak power density of 449 mW/cm^2 and a Pt utilization of 919 mW/mg_{Pt}. Time studies have shown that Pt nanoparticle synthesis is a very fast reaction. Based on our observations, we believe further catalytic improvements can be realized for 1-D carbon-supported Pt as well as the synthesis of other useful nanomaterials.

Acknowledgments

This study was supported in part by a faculty seed grant awarded to Dr. André D. Taylor by the Office of the Vice President of Research at the University of Michigan. The authors thank Harald Eberhart for useful discussions regarding the quartz reactor experiments.

References

[1] S.H. Joo, S.J. Choi, I. Oh, J. Kwak, Z. Liu, O. Terasaki, R. Ryoo, Nature 412 (2001) 169–172.
[2] F. Knowledge, Fuel Cells Durability, Stationary, Automotive, Portable: Furthering Science through Information, Knowledge Press, Brookline, MA, 2006.
[3] N. Tian, Z.Y. Zhou, S.G. Sun, Y. Ding, Z.L. Wang, Science 316 (2007) 732–735.
[4] M.S. Wilson, S. Gottesfeld, J. Electrochem. Soc. 139 (1992) L28–L30.
[5] S.A. Lee, K.W. Park, J.H. Choi, B.K. Kwon, Y.E. Sung, J. Electrochem. Soc. 149 (2002) A1299–A1304.
[6] V. Radmilovic, T.J. Richardson, S.J. Chen, P.N. Ross, J. Catal. 232 (2005) 199–209.
[7] S.D. Thompson, L.R. Jordan, M. Forsyth, Electrochim. Acta 46 (2001) 1657–1663.
[8] S. Srinivasan, O.A. Velev, A. Parthasarathy, D.J. Manko, A.J. Appleby, J. Power Sources 36 (1991) 299–320.
[9] C. Wang, M. Waje, X. Wang, J.M. Tang, R.C. Haddon, Y.S. Yan, Nano Lett. 4 (2004) 345–348.
[10] G. Girishkumar, M. Rettker, R. Underhile, D. Binz, K. Vinodgopal, P. McGinn, P. Kamat, Langmuir 21 (2005) 8487–8494.
[11] C.A. Bessel, K. Laubernds, N.M. Rodriguez, R.T.K. Baker, J. Phys. Chem. B 105 (2001) 1115–1118.
[12] E.S. Steigerwalt, G.A. Deluga, D.E. Cliffel, C.M. Lukehart, J. Phys. Chem. B 105 (2001) 8097–8101.
[13] K.J. Loh, J. Kim, J.P. Lynch, N.W.S. Kam, N.A. Kotov, Smart Mater. Struct. (2007) 429–438.
[14] J. Chen, V. Perebeinos, M. Freitag, J. Tsang, Q. Fu, J. Liu, P. Avouris, Science 310 (2005) 1171–1174.
[15] M.C. Gutierrez, Z.Y. Garcia-Carvajal, M.J. Hortiguela, L. Yuste, F. Rojo, M.L. Ferrer, F. del Monte, J. Mater. Chem. 17 (2007) 2992–2995.
[16] S. Iijima, Nature 354 (1991) 56–58.
[17] G.G. Wildgoose, C.E. Banks, R.G. Compton, Small 2 (2006) 182–193.
[18] K. Lee, J.J. Zhang, H.J. Wang, D.P. Wilkinson, J. Appl. Electrochem. 36 (2006) 507–522.
[19] E. Dujardin, T.W. Ebbesen, H. Hiura, K. Tanigaki, Science 265 (1994) 1850–1852.
[20] V. Hacker, E. Wallnofer, W. Baumgartner, T. Schaffer, J.O. Besenhard, H. Schrottner, M. Schmied, Electrochem. Commun. 7 (2005) 377–382.
[21] X.B. Fu, H. Yu, F. Peng, H.J. Wang, Y. Qian, Appl. Catal. A Gen. 321 (2007) 190–197.
[22] T. Matsumoto, Y. Nagashima, T. Yamazaki, J. Nakamura, Electrochem. Solid State Lett. 9 (2006) A160–A162.
[23] Z.L. Liu, J.Y. Lee, W.X. Chen, M. Han, L.M. Gan, Langmuir 20 (2004) 181–187.
[24] Y.T. Kim, K. Ohshima, K. Higashimine, T. Uruga, M. Takata, H. Suematsu, T. Mitani, Angew. Chem. Int. Ed. 45 (2006) 407–411.
[25] X. Sun, R. Li, D. Villers, J.P. Dodelet, S. Desilets, Chem. Phys. Lett. 379 (2003) 99–104.
[26] F.L. Yuan, H.J. Ryu, Nanotechnology 15 (2004) S596–S602.
[27] J.S. Guo, G.Q. Sun, Q. Wang, G.X. Wang, Z.H. Zhou, S.H. Tang, L.H. Jiang, B. Zhou, Q. Xin, Carbon 44 (2006) 152–157.
[28] T. Matsumoto, T. Komatsu, H. Nakano, K. Arai, Y. Nagashima, E. Yoo, T. Yamazaki, M. Kijima, H. Shimizu, Y. Takasawa, J. Nakamura, Catal. Today 90 (2004) 277–281.
[29] G.S. Duesberg, S. Roth, P. Downes, A. Minett, R. Graupner, L. Ley, N. Nicoloso, Chem. Mater. 15 (2003) 3314–3319.
[30] N. Akiya, P.E. Savage, Chem. Rev. 102 (2002) 2725–2750.
[31] C.M. Comisar, P.E. Savage, Ind. Eng. Chem. Res. 46 (2007) 1690–1695.
[32] J.V. Williams, C.N. Adams, N.A. Kotov, P.E. Savage, Ind. Eng. Chem. Res. 46 (2007) 4358–4362.
[33] K.C. Park, T. Hayashi, H. Tomiyasu, M. Endo, M.S. Dresselhaus, J. Mater. Chem. 15 (2005) 407–411.

[34] X.R. Ye, Y.H. Lin, C.M. Wang, M.H. Engelhard, Y. Wang, C.M. Wai, J. Mater. Chem. 14 (2004) 908–913.
[35] Y.H. Lin, X.L. Cui, C. Yen, C.M. Wai, J. Phys. Chem. B 109 (2005) 14410–14415.
[36] Y.H. Lin, X.L. Cui, C.H. Yen, C.M. Wai, Langmuir 21 (2005) 11474–11479.
[37] C.H. Yen, X.L. Cui, H.B. Pan, S.F. Wang, Y.H. Lin, C.M. Wai, J. Nanosci. Nanotechnol. 5 (2005) 1852–1857.
[38] A. Bayrakceken, U. Kitkamthorn, M. Aindow, C. Erkey, Scripta Mater. 56 (2007) 101–103.
[39] Z.Y. Sun, Z.M. Liu, B.X. Han, Y. Wang, J.M. Du, Z.L. Xie, G.J. Han, Adv. Mater. 17 (2005) 928.
[40] Z.Y. Sun, L. Fu, Z.M. Liu, B.X. Han, Y.Q. Liu, J.M. Du, J. Nanosci. Nanotechnol. 6 (2006) 691–697.
[41] Y. Wang, X. Xu, Z.Q. Tian, Y. Zong, H.M. Cheng, C.J. Lin, Chem. Eur. J. 12 (2006) 2542–2549.
[42] A.D. Taylor, E.Y. Kim, V.P. Humes, J. Kizuka, L.T. Thompson, J. Power Sources 171 (2007) 101–106.
[43] A.D. Taylor, M. Michel, R. Sekol, J.M. Kizuka, N.A. Kotov, L.T. Thompson, Adv. Funct. Mater. (2008), doi:10.1002/adfm.200701516, in press.
[44] M. Michel, A. Taylor, R. Sekol, P. Podsiadlo, P. Ho, N. Kotov, L. Thompson, Adv. Mater. 19 (2007) 3859–3864.
[45] B.S. Shim, J. Starkovich, N. Kotov, Compos. Sci. Technol. 66 (2006) 1174–1181.
[46] R.H. Perry, D.W. Green, Perry's Chemical Engineers' Handbook, McGraw–Hill, New York, 1997.
[47] Design Institute for Physical Properties, Sponsored by AIChE DIPPR Project 801, 2005.
[48] J.R. Lawson, M.T. Klein, Ind. Eng. Chem. Fundam. 24 (1985) 203–208.
[49] J.C. Jacquier, P.L. Desbene, J. Chromatogr. A 743 (1996) 307–314.
[50] M.F. Emerson, A. Holtzer, J. Phys. Chem. 71 (1967) 3320.